

## A thermodynamic study of shear banding in polymer solutions

Soroush Hooshyar and Natalie Germann

Citation: *Physics of Fluids* **28**, 063104 (2016); doi: 10.1063/1.4953859

View online: <http://dx.doi.org/10.1063/1.4953859>

View Table of Contents: <http://scitation.aip.org/content/aip/journal/pof2/28/6?ver=pdfcov>

Published by the [AIP Publishing](#)

---

### Articles you may be interested in

[A study of shear banding in polymer solutions](#)

*Phys. Fluids* **26**, 063101 (2014); 10.1063/1.4878842

[Shear banding in polymer solutions](#)

*Phys. Fluids* **25**, 051703 (2013); 10.1063/1.4805089

[Stability of the plane shear flow of dilute polymeric solutions](#)

*Phys. Fluids* **21**, 014109 (2009); 10.1063/1.3063893

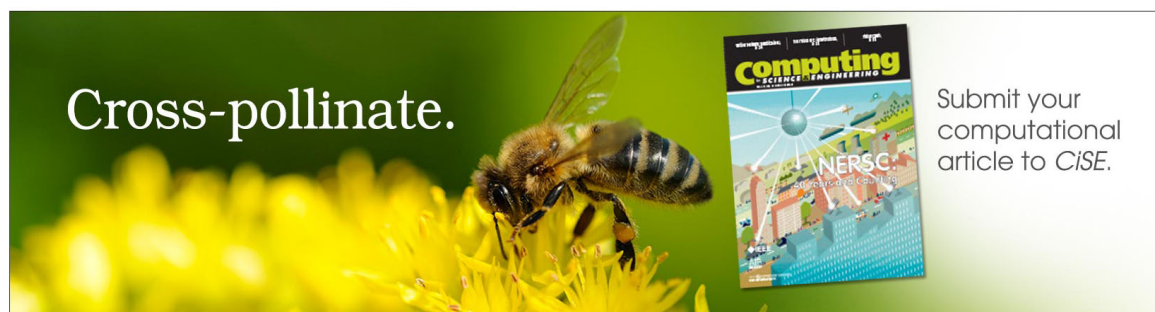
[Theory of shear-induced migration in dilute polymer solutions near solid boundaries](#)

*Phys. Fluids* **17**, 083103 (2005); 10.1063/1.2011367

[Polymer chain dynamics in dilute solution under Couette flow. II. High molecular weight poly\( \$\alpha\$ -methylstyrene\) in good solvent](#)

*J. Chem. Phys.* **114**, 9163 (2001); 10.1063/1.1365953

---

The advertisement features a close-up photograph of a bee on a yellow flower. The text 'Cross-pollinate.' is overlaid on the left. On the right, there is a small image of a journal cover titled 'Computing Science Engineering' with 'NERSC' and 'Engineering on the Edge' also visible. Below the journal cover, the text reads 'Submit your computational article to CISE.'

## A thermodynamic study of shear banding in polymer solutions

Soroush Hooshyar and Natalie Germann<sup>a)</sup>

*Fluid Dynamics of Complex Biosystems, School of Life Sciences Weihenstephan, Technical University of Munich, Freising 85354, Germany*

(Received 23 November 2015; accepted 1 June 2016; published online 21 June 2016)

Although shear banding is a ubiquitous phenomenon observed in soft materials, the mechanisms that give rise to shear-band formation are not always the same. In this work, we develop a new two-fluid model for semi-dilute entangled polymer solutions using the generalized bracket approach of nonequilibrium thermodynamics. The model is based on the hypothesis that the direct coupling between polymer stress and concentration is the driving mechanism of steady shear-band formation. To obtain smooth banded profiles in the two-fluid framework, a new stress-diffusive term is added to the time evolution equation for the conformation tensor. The advantage of the new model is that the differential velocity is treated as a state variable. This allows a straightforward implementation of the additional boundary conditions arising from the derivative diffusive terms with respect to this new state variable. To capture the overshoot of the shear stress during the start of a simple shear flow, we utilize a nonlinear Giesekus relaxation. Moreover, we include an additional relaxation term that resembles the term used in the Rouse linear entangled polymer model to account for convective constraint release and chain stretch to generate the upturn of the flow curve at large shear rates. Numerical calculations performed for cylindrical Couette flow confirm the independency of the solution from the deformation history and initial conditions. Furthermore, we find that stress-induced migration is the responsible diffusive term for steady-state shear banding. Because of its simplicity, the new model is an ideal candidate for the use in the simulation of more complex flows. *Published by AIP Publishing*. [<http://dx.doi.org/10.1063/1.4953859>]

### I. INTRODUCTION

Many soft materials can develop localized bands with different shear rates, which are known as shear bands. Although the rheology of shear-banding materials has been studied for over a decade, the different mechanisms that give rise to shear-band formation are not well understood. For a review of shear banding in complex fluids, please refer to Refs. 1–3.

The most intensively studied systems that form shear bands are worm-like micelles, which are flexible cylindrical self-assemblies of surfactant molecules in a solution. Worm-like micelles are also called living polymers because they not only relax through the same processes as polymers, including reptation and Rouse-like motion, but also break and reform reversibly. Shear banding is thought to arise in these systems from the dynamic breakage and recombination processes of the micellar species.<sup>4,5</sup> During the past decade, a few multi-species models taking these continuous processes into account have been developed using arguments from kinetic theory<sup>6</sup> and nonequilibrium thermodynamics.<sup>7,8</sup> For a constitutive model to predict shear banding in semi-dilute worm-like micellar solutions, the flow curve of the shear stress versus the applied shear rate must

---

<sup>a)</sup>[natalie.germann@tum.de](mailto:natalie.germann@tum.de)

be non-monotonic for a steady homogeneous flow. However, solutions along the decreasing part of this curve are known to be mathematically unstable. The flow therefore separates into zones with different shear rates that coexist at identical values of stress. The experimentally observed stress plateau in the region of shear banding can be recovered by including stress diffusion in the time evolution equation of the conformation/extra stress tensor.<sup>4,9</sup> Stress diffusion also guarantees a unique stress selection and, furthermore, smooths the transition region between the shear bands.<sup>4,10</sup>

In contrast, the shear stress of semi-dilute entangled polymer solutions is typically a monotonically increasing function of the shear rate. One disadvantage of the early reptation models for entangled polymers, such as the integral Doi-and-Edwards model,<sup>11</sup> is that they cannot predict a monotonic flow curve in the absence of a large solvent contribution. This is because the mechanism of convected constraint release (CCR) of the entanglements due to flow and chain stretch are missing in the description. A famous differential approximation of the Doi-and-Edwards model that includes these features is the Rouse linear entangled polymer (Rolie-Poly) model developed by Likhtman and Graham.<sup>12</sup> In a numerical study, Adams and Olmsted<sup>13</sup> showed that the Rolie-Poly model can predict transient shear banding, provided the slope of the monotonic flow curve is small enough. As steady state is achieved, the velocity profile eventually smooths out. In addition to this limitation, shear banding is obtained for much larger entanglement numbers than those found in experiments. Moreover, the high shear branch cannot be correctly described without violating certain physical criteria used to define the effect of chain stretch on CCR.<sup>14</sup> By performing a linear stability analysis within a highly general framework that encompasses the most widely used models for the rheology of shear-banding materials, which only take one fluid phase into account, Moorcroft and Fielding<sup>15</sup> provided a fluid-universal criterion for the onset of shear banding. The theoretical results were supported by the numerical predictions of the Rolie-Poly and Giesekus models.<sup>16</sup> They showed that materials that undergo a stress overshoot during the start-up of a simple shear flow have a tendency to shear band. Moreover, they found that such models are not capable of predicting steady-state bands if the flow curve is strictly monotonic. In summary, one-fluid models fail to describe polymer systems that display shear bands at steady state and, therefore, their applicability seems to be limited.

By performing rheometric tests coupled with particle-tracking velocimetry, it has been shown that highly entangled polybutadiene solutions<sup>17,18</sup> and DNA,<sup>19</sup> as a model monodisperse polymer solution, can form shear bands. Depending on the rate at which the rheometer is ramped up and the entanglement number of the polymer, the velocity profile can be linear or banded at steady state. However, these findings should be interpreted very cautiously, as entangled polymer solutions usually suffer edge fracture, so that reliable results are difficult to obtain.<sup>20</sup> Another group of researchers<sup>21,22</sup> used optical coherence tomography to record banded velocity profiles in concentrated solutions of high-molecular weight polyacrylamide at steady state. According to these authors, their data are reproducible and independent of the flow geometry used. More experimental research is required to obtain reliable and more extensive information about the shear-banding behavior in different polymeric systems.

Several experimental studies have reported that high-molecular weight polymers can form spatially inhomogeneous concentration profiles when they are subjected to shear flow.<sup>23–25</sup> Dill and Zimm<sup>23</sup> presented a new method for the separation of large DNA molecules from small ones by radial migration. In their study, they showed that when DNA molecules are sheared in a flow field between a pair of concentric cylinders or cones, they can effectively be separated. This is because the centripetal velocity toward the axis of the apparatus is a power-law function of molecular weight. In addition, Metzner *et al.*<sup>25</sup> detected migration effects across streamlines in Poiseuille flows of polymer solutions that fall between the dilute and semi-dilute concentration range. Their experimental apparatus consisted of a tube that communicates with a concentric cavity filled with the same fluid and whose inlets and outlets are connected via a loop for recirculation. After the solution was recirculated for a long time, a significant increase of polymer concentration in the stagnant cavity was found. Finally, MacDonald and Muller<sup>24</sup> performed long-term shearing measurements on a dilute polystyrene solution in a cone-and-plate geometry and used a gel permeation chromatography technique to measure the polymer concentration as a function of the radial position. The large

increase in polymer concentration near the apex of the cone and the depletion of the polymer near the edge was related to the shear-induced migration of the polymeric constituents.

The two-fluid approach is an appropriate means for describing diffusion processes in complex fluids. This method has predominantly been used in the past to study enhanced concentration fluctuations in worm-like micellar solutions,<sup>26</sup> polymer solutions,<sup>26–29</sup> and polymer melts<sup>30</sup> near the critical point of phase separation, leading to an observed increase in turbidity. This approach assumes that local gradients in the concentration and—if accounted for—viscoelastic stress generate a nontrivial velocity difference between the constituents of the mixture, which allows them to diffuse at different speeds. To the best of our knowledge, Goveas and Fredrickson<sup>31</sup> were the first researchers to use a two-fluid model to predict shear banding in a polymeric material. They considered a bidisperse polymer melt and used the well-known upper-convected Maxwell model to calculate the viscoelastic stress of each polymer species. In the 1990s, Beris and Edwards<sup>32</sup> developed a two-fluid description using the generalized bracket approach of non-equilibrium thermodynamics. Almost a decade later, Apostolakis *et al.*<sup>33</sup> used this description to investigate shear-induced migration effects in a dilute polymer solution. Unfortunately, they implemented the two-fluid approach in an *ad hoc* manner. In the resulting model, the differential velocity only appears in the time evolution equation for polymer conformation. To account for diffusion in the concentration equation, they added second-order gradient terms to this equation. If the differential velocity is assumed to vanish in the radial direction, the flow problem can be closed by imposing a no-flux condition on the polymer concentration at the solid walls and a global constraint of total mass conservation.

Based on the experimental evidence that polymer concentration can become inhomogeneous in a shear flow, Cromer *et al.*<sup>34</sup> hypothesized that shear banding in semi-dilute entangled polymer solutions is triggered by diffusion. Inspired by the kinetic theory developed by Goveas and Fredrickson,<sup>31</sup> these authors recently developed a two-fluid model for shear-banding polymer solutions.<sup>35</sup> Their model was obtained by considering only one type of polymer dissolved in a viscous solvent and replacing the Johnson–Segalman model with the Rolie–Poly model. Because this model accounts for chain stretch and convective constraint release, the polymer stress can be predicted more reliably under rapid deformations. In contrast to Apostolakis *et al.*,<sup>33</sup> they introduced diffusive terms in the time evolution equation for the polymer concentration in a consistent manner. To ensure that the polymer concentration remains conserved, they had to impose a no-flux condition at the solid boundaries. The remaining boundary conditions were constructed so that the differential velocity vanishes at the boundaries.<sup>35,36</sup>

As observed by Beris and Mavrantzas,<sup>37</sup> different theoretical frameworks can lead to similar macroscopic equations governing the direct coupling between concentration and viscoelastic fluid flow. By combining a two-fluid description with a realistic constitutive model for the extra stress, Cromer *et al.*<sup>34</sup> were the first to predict steady-state shear banding for systems that display a monotonic flow curve. Their polymer model can predict important features, such as the independence of the solution from the deformation history and initial condition, the occurrence of a banded steady state if the flow is ramped quickly enough from rest, the characteristic long-lived transients of shear-banding fluids, and elastic recoil after fast deformations. By means of a linear stability analysis, Cromer *et al.*<sup>36</sup> showed that in opposition to Fickian diffusion, shear-induced migration can force polymers to increase their concentration gradients, thereby creating a shear banding instability for a certain range of parameters. Furthermore, they found that the ratio of the polymer correlation length to the channel width determines the number of bands in planar shear flow. Subsequently, Cromer *et al.*<sup>36</sup> incorporated thermal noise in their two-fluid framework through a canonical Langevin approach to investigate concentration fluctuations in semi-dilute entangled polymer solutions under extensional flow. To prevent divergence in extensional flow, they modified the Rolie–Poly model with a finitely extensible non-linear elastic-type chain stretch limitation. For the first time, the finite-wavelength concentration fluctuation amplification observed experimentally by van Egmond and Fuller<sup>38</sup> could be predicted. In summary, these recent studies highlight the importance of accounting for diffusional effects. Moreover, they confirm that a reliable time evolution equation for the conformation/extra stress tensor is required in order to be able to reliably predict phenomena that are related to the coupling between polymer stress and concentration.

Germann *et al.*<sup>5</sup> improved the two-fluid framework for viscoelastic fluids developed by Beris and Edwards<sup>32</sup> using the generalized bracket approach of nonequilibrium thermodynamics. This new formulation is advantageous because the total mass is conserved by the time evolution equations themselves. Consequently, it can easily be applied to viscoelastic systems comprising more than two phases. In addition, it is no longer necessary to impose a no-flux condition on the polymer concentration in order to prevent the outflow of material through the system boundaries. As in all other previous approaches, the differential velocity was considered to be an intermediate variable, which complicates the specifications of the additional boundary conditions arising from the higher-order diffusive terms. To overcome this difficulty, the same authors suggested treating the differential velocity as a state variable.<sup>39</sup> Consequently, the additional boundary conditions arising from the derivative diffusive terms can be imposed directly with respect to this new state variable. For instance, no-slip and no-flux boundary conditions translate into the requirements that the tangential and normal components, respectively, of the differential velocity must vanish at the boundaries. Overall, this work is a significant contribution because it lays the foundation for a proper mathematical formulation of advection–diffusion problems.

The goal of the present work is to adopt the two-fluid approach developed by Germann *et al.*<sup>5,39</sup> to describe shear banding in semi-dilute entangled polymer solutions. In the time evolution equation for the conformation tensor, a nonlinear Giesekus relaxation is used to capture the overshoot occurring during a rapid start-up of a simple shearing flow, shear-thinning behavior, and nontrivial first and second normal stress differences. We believe that the Giesekus relaxation is an appropriate choice, as it was originally derived from dumbbell kinetic theory using hydrodynamic drag and Brownian motion to account for the interactions between the polymeric constituents in a concentrated solution or melt. In addition, we include a second nonlinear relaxation term to describe the monotonic growth of the shear stress at large shear rates. This term is similar to the one used in the Rolie–Poly model to account for CCR and chain stretch.<sup>12</sup> The Rolie–Poly model was not considered here to describe the conformational dynamics, as the CCR term of this model cannot be derived within the framework of nonequilibrium thermodynamics. Leygue *et al.*<sup>40</sup> developed an expression for CCR using the generalized bracket approach of nonequilibrium thermodynamics. However, like the Marrucci-Gregio-Ianniruberto model,<sup>40</sup> this model does not consider chain stretching. Moreover, because of the strain measure used, it cannot be easily incorporated in the two-fluid approach of Germann *et al.*<sup>5,39</sup>

The remainder of this paper is organized as follows. Sec. II presents the two-fluid approach used to develop a new model for semi-dilute entangled polymer solutions. Sec. III analyzes the behavior of the model for a circular Couette flow. Sec. IV presents the conclusions.

## II. POLYMER MODEL

In this work, the two-fluid approach proposed by Germann *et al.*<sup>5,39</sup> is adopted to develop a model for semi-dilute entangled polymeric solutions. We consider the total system to be closed, isothermal, and incompressible. This system consists of two components: one species of polymeric constituents and a viscous solvent. For the polymeric species, the following state variables are defined: mass density  $\rho_p$ ; momentum density  $\mathbf{m}^p = \rho_p \mathbf{v}^p$ , where  $\mathbf{v}^p$  is the velocity field; and structural tensorial parameter density  $\mathbf{C} = n_p \mathbf{c}$ , where  $n_p$  is the number density and  $\mathbf{c}$  is the conformation tensor. The number density of the polymer component is given by  $n_p = (\rho_p/M_p)N_A$ , where  $M_p$  is the molecular weight of the polymer and  $N_A$  is the Avogadro constant. For the viscous solvent, we define the following state variables: mass density  $\rho_s = n_s M_s/N_A$ , where  $n_s$  denotes the number density of the solvent and  $M_s$  its molecular weight, and momentum density  $\mathbf{m}^s = \rho_s \mathbf{v}^s$ , where  $\mathbf{v}^s$  is the velocity field. The total mass of the polymeric solution is  $\rho = \rho_p + \rho_s$ . Within the bracket formalism of non-equilibrium thermodynamics,<sup>32</sup> the system dynamics are described by the master equation

$$\frac{dF}{dt} = \{F, H\} + [F, H], \quad (1)$$

where  $F$  is an arbitrary functional depending on the system variables and  $H$  is the Hamiltonian or total system energy. The Poisson bracket  $\{\cdot, \cdot\}$  and dissipation bracket  $[\cdot, \cdot]$  represent the reversible and irreversible contributions, respectively, to the system dynamics. The total system energy is characterized by the following components of the Hamiltonian:

$$H = H_k + H_e + H_m, \quad (2)$$

where

$$H_k = \int_{\Omega} \frac{1}{2} \left( \frac{\mathbf{m}^p \cdot \mathbf{m}^p}{\rho_p} + \frac{\mathbf{m}^s \cdot \mathbf{m}^s}{\rho_s} \right) d^3x, \quad (3)$$

$$H_e = \int_{\Omega} \frac{1}{2} \left\{ K \text{tr} \mathbf{C} - n_p k_B T \ln \det \left( \frac{K \mathbf{C}}{n_p k_B T} \right) \right\} d^3x, \quad (4)$$

$$H_m = \int_{\Omega} \left\{ n_p k_B T \ln \left( \frac{\rho_p}{\rho_p + \rho_s} \right) + n_s k_B T \ln \left( \frac{\rho_s}{\rho_p + \rho_s} \right) \right\} d^3x. \quad (5)$$

Here,  $\Omega$  is the flow domain,  $K$  is the Hookean spring constant associated with the polymer,  $k_B$  is the Boltzmann constant, and  $T$  is the absolute temperature. Eq. (3) represents contributions of the solvent and the polymeric constituents to the kinetic energy, Eq. (4) represents the elastic free energy associated with the Hookean dumbbells of the polymers, and Eq. (5) is the standard Flory-Huggins entropy of random mixing. For simplicity, we do not consider any dependence of the total system energy on gradients in the state variables. Differentiating the Hamiltonian with respect to the momentum densities of the polymer and solvent yields  $\delta H / \delta \mathbf{m}^p = \mathbf{m}^p / \rho_p = \mathbf{v}^p$  and  $\delta H / \delta \mathbf{m}^s = \mathbf{m}^s / \rho_s = \mathbf{v}^s$ , respectively.

For the given set of state variables, the Poisson bracket can be constructed as follows:<sup>32</sup>

$$\begin{aligned} \{F, H\} = & - \int_{\Omega} \left\{ \frac{\delta F}{\delta \rho_p} \nabla_{\beta} \left( \frac{\delta H}{\delta m_{\beta}^p} \rho_p \right) - \frac{\delta H}{\delta \rho_p} \nabla_{\beta} \left( \frac{\delta F}{\delta m_{\beta}^p} \rho_p \right) \right\} d^3x \\ & - \int_{\Omega} \left\{ \frac{\delta F}{\delta m_{\gamma}^p} \nabla_{\beta} \left( \frac{\delta H}{\delta m_{\beta}^p} m_{\gamma}^p \right) - \frac{\delta H}{\delta m_{\gamma}^p} \nabla_{\beta} \left( \frac{\delta F}{\delta m_{\beta}^p} m_{\gamma}^p \right) \right\} d^3x \\ & - \int_{\Omega} \left\{ \frac{\delta F}{\delta C_{\alpha\beta}} \nabla_{\gamma} \left( \frac{\delta H}{\delta m_{\gamma}^p} C_{\alpha\beta} \right) - \frac{\delta H}{\delta C_{\alpha\beta}} \nabla_{\gamma} \left( \frac{\delta F}{\delta m_{\gamma}^p} C_{\alpha\beta} \right) \right\} d^3x \\ & - \int_{\Omega} C_{\alpha\gamma} \left( \frac{\delta H}{\delta C_{\alpha\beta}} \nabla_{\gamma} \frac{\delta F}{\delta m_{\beta}^p} - \frac{\delta F}{\delta C_{\alpha\beta}} \nabla_{\gamma} \frac{\delta H}{\delta m_{\beta}^p} \right) d^3x \\ & - \int_{\Omega} C_{\beta\gamma} \left( \frac{\delta H}{\delta C_{\alpha\beta}} \nabla_{\gamma} \frac{\delta F}{\delta m_{\alpha}^p} - \frac{\delta F}{\delta C_{\alpha\beta}} \nabla_{\gamma} \frac{\delta H}{\delta m_{\alpha}^p} \right) d^3x \\ & - \int_{\Omega} \left\{ \frac{\delta F}{\delta \rho_s} \nabla_{\beta} \left( \frac{\delta H}{\delta m_{\beta}^s} \rho_s \right) - \frac{\delta H}{\delta \rho_s} \nabla_{\beta} \left( \frac{\delta F}{\delta m_{\beta}^s} \rho_s \right) \right\} d^3x \\ & - \int_{\Omega} \left\{ \frac{\delta F}{\delta m_{\gamma}^s} \nabla_{\beta} \left( \frac{\delta H}{\delta m_{\beta}^s} m_{\gamma}^s \right) - \frac{\delta H}{\delta m_{\gamma}^s} \nabla_{\beta} \left( \frac{\delta F}{\delta m_{\beta}^s} m_{\gamma}^s \right) \right\} d^3x. \end{aligned} \quad (6)$$

Without any dissipation, the time evolution equations for the state variables are

$$\frac{\partial \rho_p}{\partial t} = -\nabla_{\alpha} (v_{\alpha}^p \rho_p), \quad (7)$$

$$\frac{\partial \rho_s}{\partial t} = -\nabla_{\alpha} (v_{\alpha}^s \rho_s), \quad (8)$$

$$\begin{aligned} \frac{\partial}{\partial t} (\rho_p v_{\alpha}^p) = & -\nabla_{\beta} (v_{\beta}^p \rho_p v_{\alpha}^p) - m_{\beta}^p \nabla_{\alpha} \left( \frac{\delta H}{\delta m_{\beta}^p} \right) \\ & - \rho_p \nabla_{\alpha} \left( \frac{\delta H}{\delta \rho_p} \right) - C_{\beta\gamma} \nabla_{\alpha} \left( \frac{\delta H}{\delta C_{\beta\gamma}} \right) + \nabla_{\beta} \sigma_{\beta\alpha}^p, \end{aligned} \quad (9)$$

$$\frac{\partial}{\partial t} (\rho_s v_\alpha^s) = -\nabla_\beta (v_\beta^s \rho_s v_\alpha^s) - \rho_s \nabla_\alpha \left( \frac{\delta H}{\delta \rho_s} \right) - m_\beta^s \nabla_\alpha \left( \frac{\delta H}{\delta m_\beta^s} \right), \quad (10)$$

$$\frac{\partial C_{\alpha\beta}}{\partial t} = -\nabla_\gamma (v_\gamma^p C_{\alpha\beta}) + C_{\gamma\alpha} \nabla_\gamma v_\beta^p + C_{\gamma\beta} \nabla_\gamma v_\alpha^p, \quad (11)$$

where  $\sigma^P$  denotes the extra stress associated with the polymer, which is defined as

$$\sigma_{\alpha\beta}^P \equiv 2C_{\alpha\gamma} \frac{\delta H}{\delta C_{\gamma\beta}} = KC_{\alpha\beta} - n_p k_B T \delta_{\alpha\beta}. \quad (12)$$

To incorporate the incompressibility constraint corresponding to a constant total mass density, it is necessary to switch to a new set of variables. Let the mass average velocity be defined as

$$\mathbf{v} \equiv \frac{\rho_p}{\rho} \mathbf{v}^p + \frac{\rho_s}{\rho} \mathbf{v}^s, \quad (13)$$

and the differential velocity be defined as

$$\Delta \mathbf{v} \equiv \mathbf{v}^p - \mathbf{v}^s. \quad (14)$$

Correspondingly, the total momentum density is given as

$$\mathbf{m} \equiv \mathbf{m}^p + \mathbf{m}^s, \quad (15)$$

and the differential momentum density is given as

$$\Delta \mathbf{m} \equiv \frac{\rho_s}{\rho} \mathbf{m}^p - \frac{\rho_p}{\rho} \mathbf{m}^s = \rho_{red} \Delta \mathbf{v}. \quad (16)$$

Here,  $\rho_{red} = \rho_s \rho_p / \rho$  corresponds to the reduced mass density of the polymeric solution. The kinetic contribution to the Hamiltonian must be re-expressed as

$$H_k = \int_\Omega \frac{1}{2} \left( \frac{\mathbf{m} \cdot \mathbf{m}}{\rho} + \frac{\Delta \mathbf{m} \cdot \Delta \mathbf{m}}{\rho_{red}} \right) d^3x. \quad (17)$$

Differentiating the kinetic part of the Hamiltonian provided above yields  $\delta H_k / \delta \mathbf{m} = \delta H / \delta \mathbf{m} = \mathbf{v}$  and  $\delta H_k / \delta (\Delta \mathbf{m}) = \delta H / \delta (\Delta \mathbf{m}) = \Delta \mathbf{v}$ . As in the Newtonian case, the time evolution equation of the total momentum density can be obtained by adding those of the individual phase momentum densities. That is, if we add Eqs. (9) and (10) and then use the continuity Eqs. (7) and (8), we obtain the following time evolution equation for the total momentum density:

$$\rho \frac{\partial v_\alpha}{\partial t} = -\rho v_\beta \nabla_\beta v_\alpha - \nabla_\alpha p + \nabla_\beta \sigma_{\beta\alpha}^P, \quad (18)$$

where the thermodynamic pressure is defined as usual as

$$p \equiv -h + \rho_s \frac{\delta H}{\delta \rho_s} + m_\beta^s \frac{\delta H}{\delta m_\beta^s} + m_\beta^p \frac{\delta H}{\delta m_\beta^p} + \rho_p \frac{\delta H}{\delta \rho_p} + C_{\beta\gamma} \frac{\delta H}{\delta C_{\beta\gamma}}.$$

Here,  $h$  represents the total local free energy density, defined as  $H = \int_\Omega h d^3x$ . The viscoelasticity that appears in Eq. (18) is a dissipative contribution in the form of the divergence of the extra stress on the right-hand side. Similarly, adding the continuity Eqs. (7) and (8) together obtains

$$\frac{\partial \rho}{\partial t} = -\nabla_\alpha (v_\alpha \rho). \quad (19)$$

If we further assume that the total mass density of the polymeric solution remains, like that of most liquids, nearly constant, this equation simplifies to the well-known divergence-free constraint

$$\nabla_\alpha v_\alpha = 0. \quad (20)$$

Consequently, it is no longer necessary to calculate the pressure via Eq. (19). The pressure here is simply a projector operator of the velocity derivative in divergence-free space. If we subtract Eq. (9) from (10), multiply the first by  $\rho_s / \rho_p$  and the second by  $\rho_p / \rho_s$ , and then make use of the continuity Eqs. (7) and (8), we obtain a time evolution equation for the differential velocity. By ignoring all

inertial terms that are proportional to the square of the differential velocity, this equation becomes

$$\begin{aligned} \frac{\rho_p \rho_s}{\rho} \frac{\partial \Delta v_\alpha}{\partial t} = & -\frac{\rho_p \rho_s}{\rho} v_\beta \nabla_\beta \Delta v_\alpha + \frac{\rho_s}{\rho} \left\{ -m_\beta^p \nabla_\alpha \left( \frac{\delta H}{\delta m_\beta^p} \right) \right. \\ & \left. - \rho_p \nabla_\alpha \left( \frac{\delta H}{\delta \rho_p} \right) - C_{ij} \nabla \left( \frac{\delta H}{\delta C_{ij}} \right) + \nabla \cdot \sigma^p \right\} \\ & - \frac{\rho_p}{\rho} \left\{ -\rho_s \nabla_\alpha \left( \frac{\delta H}{\delta \rho_s} \right) - m_\beta^s \nabla_\alpha \left( \frac{\delta H}{\delta m_\beta^s} \right) \right\}. \end{aligned} \quad (21)$$

In the above equation, the higher order inertial terms have been ignored to obtain a simplified expression of the substantial derivative. We believe that the first-order approximation is justified for slow flows. As polymers in semi-dilute solutions have low inertia because of their small volume fraction, they follow the motion of the ambient solvent quickly under the action of large drag forces.

Next, we supplement Eq. (21) with the dissipative contributions to the system dynamics. An additional term accounting for the viscous drag between the polymer constituents and viscous solvent must be included in the system dynamics, i.e.,

$$[F, H] = - \int_{\Omega} Z_{\alpha\beta} \frac{\delta F}{\delta (\Delta m_\alpha)} \frac{\delta H}{\delta (\Delta m_\beta)} d^3x, \quad (22)$$

where the drag coefficient tensor  $Z_{\alpha\beta}$  is approximated by an isotropic tensor  $G_0/D\delta_{\alpha\beta}$ , where  $G_0 = n_p^0 k_B T$  is the modulus of elasticity evaluated at the linear viscoelastic limit and  $D$  is the scalar diffusivity. In addition, we can describe the viscous dissipation as follows:

$$[F, H] = - \int_{\Omega} \frac{\eta_s}{2} \left\{ \nabla_\alpha \left( \frac{\delta F}{\delta m_\beta^s} \right) + \nabla_\beta \left( \frac{\delta F}{\delta m_\alpha^s} \right) \right\} \left\{ \nabla_\alpha \left( \frac{\delta H}{\delta m_\beta^s} \right) + \nabla_\beta \left( \frac{\delta H}{\delta m_\alpha^s} \right) \right\} d^3x, \quad (23)$$

where  $\eta_s$  denotes the Newtonian solvent viscosity. To further simplify the time evolution equation for the differential velocity, we neglect the inertial contributions to the chemical potential in Eq. (21) and obtain

$$\begin{aligned} \frac{\rho_p \rho_s}{\rho} \left( \frac{\partial}{\partial t} + \mathbf{v} \cdot \nabla \right) (\Delta \mathbf{v}) = & \frac{\rho_s}{\rho} \left\{ -\nabla (n_p k_B T) + \nabla \cdot \sigma^p \right\} \\ & - \frac{\rho_p}{\rho} \left\{ -\nabla (n_s k_B T) + \eta_s \nabla^2 \mathbf{v}^s \right\} - \frac{G_0}{D} \Delta \mathbf{v}, \end{aligned} \quad (24)$$

where the local diffusivity constant  $D$  controls the diffusion between the solvent and polymer. At the diffusionless limit, i.e., if we let  $D \rightarrow 0$ , we obtain  $\Delta \mathbf{v} \rightarrow 0$ . Fickian diffusion is described by the spatial gradients of the number densities associated with the polymer and solvent; the divergence of  $\sigma^p$  accounts for stress-induced migration. Because the differential velocities are now treated as state variable, we can directly impose the additional boundary conditions arising from the presence of diffusive derivative terms appearing in Eq. (24) with respect to this variable. For instance, if we assume no slip occurs along the solid walls, we simply have to force the normal component of the differential velocity to vanish there. Furthermore, no material flux is enforced by requiring the tangential component of the differential velocity to vanish. This mathematical treatment is now possible because the Laplacian of the differential velocity implicitly appears on the right-hand side of Eq. (24). In summary, by considering the differential velocity as state variable, the additional boundary conditions can be formulated in a mathematically correct and straightforward way. This will be especially important when considering slip along the walls and flows in more complicated geometries.

Next, let us model the irreversible conformational dynamics. Below a critical value of the shear stress versus shear rate slope, the solution may not be smooth, even if the flow curve is monotonic. There are several ways to avoid this type of discontinuity. The standard approach is to add stress diffusion to the time evolution equation of the conformation/extra stress tensor.<sup>41</sup> Another approach is to include a square-gradient approximation in the mixing free energy to account for size effects.<sup>35</sup> This type of regularization is weakly nonlocal, i.e., only neighboring points are notably affected by this modification, and it has made no significant difference in our case. Therefore, we follow the



standard approach and construct a new expression for stress diffusion using the generalized bracket approach of nonequilibrium thermodynamics. The new expression is based on the one used by Beris and Edwards<sup>32</sup> to account for stress diffusion in one-fluid models.

$$[F, H_m] = - \int_{\Omega} B_{\alpha\beta} \left( \nabla_{\gamma} \left( C_{\gamma\lambda} \frac{\delta F}{\delta C_{\lambda\alpha}} \right) \right) \left( \nabla_{\varepsilon} \left( C_{\varepsilon\kappa} \frac{\delta H}{\delta C_{\kappa\beta}} \right) \right) d^3x - \int_{\Omega} B_{\alpha\beta} \left( \nabla_{\gamma} \left( C_{\gamma\lambda} \frac{\delta H}{\delta C_{\lambda\alpha}} \right) \right) \left( \nabla_{\varepsilon} \left( C_{\varepsilon\kappa} \frac{\delta F}{\delta C_{\kappa\beta}} \right) \right) d^3x, \quad (25)$$

where  $B_{\alpha\beta}$  is a second-order transport coefficient. For simplicity, we only consider isotropic transport coefficients, which leads to  $B_{\alpha\beta} = 2D_{nonloc}\delta_{\alpha\beta}$ . To obtain an expression that satisfies material objectivity, however, it is necessary to supplement the expression with the second term on the right-hand side of Eq. (25). Furthermore, we include the standard expressions for a viscoelastic system in the dissipative dynamics.<sup>32</sup> Ignoring the entropy correction terms leads to

$$[F, H_m] = - \int_{\Omega} \Lambda_{\alpha\beta\gamma\varepsilon}^1 \frac{\delta F}{\delta C_{\alpha\beta}} \frac{\delta H_m}{\delta C_{\gamma\varepsilon}} d^3x - \int_{\Omega} \Lambda_{\alpha\beta\gamma\varepsilon}^2 \frac{\delta F}{\delta C_{\alpha\beta}} \frac{\delta H_m}{\delta C_{\gamma\varepsilon}} d^3x, \quad (26)$$

where  $\Lambda_{\alpha\beta\gamma\varepsilon}^1$  and  $\Lambda_{\alpha\beta\gamma\varepsilon}^2$  are general fourth-order relaxation tensors. The first integral on the right-hand side of Eq. (26) accounts for a nonlinear Giesekus relaxation, where its phenomenological relaxation matrix is given by

$$\Lambda_{\alpha\beta\gamma\varepsilon}^1 = \frac{1}{2\lambda_1 K} [(1 - \alpha)(C_{\alpha\gamma}\delta_{\beta\varepsilon} + C_{\beta\gamma}\delta_{\alpha\varepsilon} + C_{\alpha\varepsilon}\delta_{\beta\gamma} + C_{\beta\varepsilon}\delta_{\alpha\gamma}) + 2\alpha \frac{K}{k_B T} (c_{\alpha\gamma}C_{\beta\varepsilon} + c_{\alpha\varepsilon}C_{\beta\gamma})]. \quad (27)$$

Here,  $\lambda_1$  is a characteristic relaxation time, and  $\alpha$  is the mobility factor, which relates to the anisotropic relaxation of the polymer chains. At  $\alpha = 0$ , we can recover the Maxwellian relaxation. The Giesekus relaxation term takes into account hydrodynamic drag and Brownian motion. Furthermore, it accounts for shear thinning behavior and nontrivial first and second normal stress differences. As this relaxation generates an overshoot during the start-up of a simple shearing flow, shear-band formation can be triggered. The second integral on the right-hand side of Eq. (26) has been added to model the flow curve at high shear rates. As the upturn of the shear stress at high shear rates can only be described using a second nonlinear relaxation term taking the extension of the polymeric constituents into account, we selected the following phenomenological relaxation matrix:

$$\Lambda_{\alpha\beta\gamma\varepsilon}^2 = \frac{\left[ \text{tr} \left( \frac{K}{k_B T} \mathbf{c} \right) - 3 \right]^q}{2\lambda_2 K} (C_{\alpha\gamma}\delta_{\beta\varepsilon} + C_{\beta\gamma}\delta_{\alpha\varepsilon} + C_{\alpha\varepsilon}\delta_{\beta\gamma} + C_{\beta\varepsilon}\delta_{\alpha\gamma}), \quad (28)$$

where  $\lambda_2$  denotes a characteristic relaxation time. Prefactor  $[K/(k_B T)\text{trc} - 3]^q$  depends on the trace of the conformation tensor, as it is a relative measure of polymer stretch. As the final time evolution equation of the conformation tensor provided in Eq. (31) shows, the second relaxation term resembles the term used in the Rolie-Poly model to describe CCR including chain stretch. Because we assume  $\lambda_2 \gg \lambda_1$ , parameters  $\lambda_1$  and  $\lambda_2$  can be identified as the reptation time and Rouse time, respectively.

To reduce numerical errors in the calculation of an inhomogeneous flow, we use  $\mathbf{c}$  as the unknown variable in the final model rather than  $\mathbf{C}$ . Following the standard procedure of the generalized bracket approach,<sup>32</sup> the time evolution equations for the other state variables can be identified. This is typically done by comparing the left- and right-hand sides of the master Eq. (1) after the explicit expressions of the Poisson and dissipation brackets have been inserted. Finally, we obtain

$$\rho \frac{\partial \mathbf{v}}{\partial t} = -\rho \mathbf{v} \cdot \nabla \mathbf{v} - \nabla p + \nabla \cdot \boldsymbol{\sigma}, \quad (29)$$

$$\frac{\partial n_p}{\partial t} = -\nabla \cdot (\mathbf{v}^p n_p), \quad (30)$$

$$\begin{aligned}
\frac{\partial \mathbf{c}}{\partial t} = & -\mathbf{v}^p \cdot \nabla \mathbf{c} + \mathbf{c} \cdot \nabla \mathbf{v}^p + (\nabla \mathbf{v}^p)^T \cdot \mathbf{c} \\
& - \frac{1}{\lambda_1} \left[ (1 - \alpha) \mathbf{I} + \alpha \frac{K}{k_B T} \mathbf{c} \right] \cdot \left( \mathbf{c} - \frac{K}{k_B T} \mathbf{I} \right) \\
& + \frac{1}{\lambda_2} \left[ \text{tr} \left( \frac{K}{k_B T} \mathbf{c} \right) - 3 \right]^q \left( \mathbf{c} - \frac{K}{k_B T} \mathbf{I} \right) \\
& + D_{nonloc} \left( \mathbf{c} \cdot \nabla (\nabla \cdot \boldsymbol{\sigma}^p) + [\nabla (\nabla \cdot \boldsymbol{\sigma}^p)]^T \cdot \mathbf{c} \right). \quad (31)
\end{aligned}$$

Eq. (29) is the Cauchy momentum balance, where  $p$  represents the pressure and  $\boldsymbol{\sigma}$  the extra stress tensor associated with the polymer solution. The last term on the right-hand side is the Newtonian stress. Eq. (30) is the time evolution equation for the number density of the polymer. The left-hand side and the term on the right-hand side constitute the material derivative. This equation accounts for the fact that the number density is allowed to vary locally. Eq. (31) is the time evolution equation for the conformation of the polymer. The partial time derivative on the left-hand side and the first three terms on the right-hand side constitute the upper-convected time derivative of the conformation tensor. Note that this upper-convected time derivative involves the velocity of the polymer, which can be calculated from the total and differential velocities using Eq. (33). The two-fluid approach used here can be applied in the context of viscoelastic fluids, as it allows a direct coupling between the conformational dynamics and diffusional processes. The fourth term involving parameter  $\alpha$  accounts for the Giesekus relaxation. This term generates an overshoot of the shear stress during the start-up of a simple shearing flow and thus triggers the shear-band formation. Furthermore, it accounts for shear-thinning behavior and nontrivial first and second normal stress differences. The fifth term, involving pre-factor  $[K/(k_B T)\text{tr} \mathbf{c} - 3]^q$ , is a second nonlinear relaxation term. This term has been added to generate the upturn of the flow curve at high shear rates. The prefactor depends on the trace of the conformation tensor because it is a relative measure of polymer stretch. At the linear viscoelastic limit, i.e., at low shear rates, this term vanishes. Note that this term resembles the term used in the Rolie-Poly model to account for CCR and chain stretch. Parameter  $D_{nonloc}$ , appearing in the last term of Eq. (31), controls the smoothness of the profiles.

Because of the presence of the higher-order derivatives in the last term of Eq. (31), this equation requires special treatment at the boundaries.<sup>39</sup> Because of local surface effects, diffusion should vanish at these locations within a distance of less than the gyration radius; this is because a flat “pancake” conformation is required to fit next to the rigid walls. We therefore set parameter  $D_{nonloc}$  equal to zero on the boundaries. Using this approach, it is not necessary to impose extra boundary conditions and thus make some unnecessary assumptions regarding the internal microstructure of the polymer.

Furthermore, note the similarities between the stress diffusive terms appearing in Eqs. (24) and (31). In the absence of inertia, an explicit expression for the differential velocity can be obtained from Eq. (24). Inserting this expression into Eq. (31) yields stress diffusive terms with the same structure as those that we added.

The above set of time evolution Eqs. (24) and (29)–(31) is closed by an explicit expression for the extra stress

$$\boldsymbol{\sigma} = \boldsymbol{\sigma}^p + \eta_s \left[ \nabla \mathbf{v}^s + (\nabla \mathbf{v}^s)^T \right] = n_p (K \mathbf{c} - k_B T \mathbf{I}) + \eta_s \left[ \nabla \mathbf{v}^s + (\nabla \mathbf{v}^s)^T \right], \quad (32)$$

where the first term accounts for the viscoelastic contribution of the polymer and the second term accounts for the extra stress associated with the viscous solvent.

The phase velocities appearing in the time evolution Eqs. (24) and (29)–(31) can be calculated from the total average velocity and differential velocities as follows:

$$\mathbf{v}^p = \mathbf{v} + \frac{\rho_s}{\rho} \Delta \mathbf{v}, \quad (33)$$

$$\mathbf{v}^s = \mathbf{v} - \frac{\rho_p}{\rho} \Delta \mathbf{v}. \quad (34)$$

In the equilibrium state of rest ( $\mathbf{v} = 0$  and  $\Delta \mathbf{v} = 0$ ), we can obtain the analytical solution of  $n_p = n_p^0$  and  $\mathbf{c} = (k_B T / K) \mathbf{I}$ .

### A. Non-dimensionalization

In the following, we work with dimensionless quantities. The spatial position is scaled by the characteristic height  $\tilde{\mathbf{x}} = \mathbf{x} / H$ ; time is scaled by the characteristic relaxation time  $\tilde{t} = t / \lambda_1$ ; pressure is scaled by the plateau modulus  $\tilde{p} = p / G_0$ ; extra stress is scaled as  $\tilde{\boldsymbol{\sigma}} = \boldsymbol{\sigma} / G_0$ ; the conformation tensor associated with the polymer is scaled as  $\tilde{\mathbf{c}} = (K / k_B T) \mathbf{c}$ ; and the number density of component  $i = p, s$  is scaled as  $\tilde{n}_i = n_i / n_p^0$ . The dimensionless parameters with respect to these scalings are the elasticity number  $E = G_0 \lambda_1^2 / \rho H^2$ ; the ratio of the molecular weight of the solvent to that of the polymer  $\chi = M_s / M_p$ ; the viscosity ratio  $\beta = \eta_s / \eta_0$ , where  $\eta_0 = G_0 \lambda_1$  is the zero shear viscosity; and the ratio of the two characteristic relaxation times  $\varepsilon = \lambda_1 / \lambda_2$ . By assuming an initially uniform polymer concentration in the flow field, the total polymer concentration can be calculated as  $\mu = \tilde{n}_p^0 / (\tilde{n}_p^0 + \chi \tilde{n}_s^0)$ . The non-dimensional diffusion coefficients are defined as  $\tilde{D} = D \lambda_1 / H^2$  and  $\tilde{D}_{nonloc} = D_{nonloc} \lambda_1 / H^2$ . The non-dimensionalized form of the model Eqs. (24) and (29)–(34) can be found in [Appendix](#).

## III. RESULTS

In this section, we analyze the behavior of the new model comprising time evolution Eqs. (24) and (29)–(31), the explicit expression of the extra stress tensor provided in Eq. (32), and the explicit expressions of the phase velocities provided in Eqs. (33) and (34) in shear flow. We consider the flow in the annular gap between two concentric cylinders. The inner cylinder rotates in the counter-clockwise direction while the outer cylinder is kept stationary. The characteristic height is given as  $H = R_o - R_i$ , where  $R_o$  and  $R_i$  represent the radii of the outer and inner cylinders, respectively. The dimensionless curvature  $q^* = (R_o - R_i) / R_i$  specifies the relative position of the cylinders. The cylindrical coordinate system was used as the reference frame with  $r$ ,  $\theta$ , and  $z$  for the radial, azimuthal, and axial coordinates, respectively. Normalized coordinate  $\tilde{r}^* = (r - R_i) / (R_o - R_i)$  is employed to indicate the location in the gap.

### A. Steady homogeneous shear flow

To study the effect of the CCR-like term, we first consider the special case of steady homogeneous shear flow. As the values of the model parameters are typically determined under homogeneous shear flow conditions, this type of flow is of relevance. Homogeneous shear flow can be obtained by neglecting the cylindrical curvature and assuming the shear rate across the gap to be constant. Under this condition, the differential velocity is identically zero and the new model reduces to the standard Giesekus model for  $\varepsilon = 0$ .

The parameter values of the new and Giesekus models were determined by manually fitting these models to the flow curve obtained for a 10 wt./wt. % (1.6M) shear-banding polybutadiene solution.<sup>18</sup> The parameters of the new model that have an influence on the shape of the flow curve and thus are determined by the fitting process are mobility factor  $\alpha = 0.73$ , ratio of the characteristic relaxation times  $\varepsilon = 2.5 \times 10^{-4}$ , power-law parameter  $q = 1.46$ , and viscosity ratio  $\beta = 10^{-5}$ . For the Giesekus model, we obtain mobility factor  $\alpha = 0.73$  and viscosity ratio  $\beta = 8 \times 10^{-4}$ . The governing sets of algebraic flow equations were solved using Newton's method with lower-upper triangular decomposition.<sup>42</sup>

We compare the flow curves predicted by the new model and its limiting case, i.e., the Giesekus model, with experimental data.<sup>18</sup> Fig. 1 displays the absolute value of the shear stress as a function of the dimensionless shear rate or Weissenberg number,  $Wi \equiv \tilde{\gamma} = \lambda_1 V / H$ . As the Giesekus relaxation dominates over the CCR-like term at small and medium shear rates, the predictions of the two models coincide in this flow regime. Because of the presence of the CCR-like term, our model can capture the upturn of the curve without the need for a solvent contribution. Additionally, it is

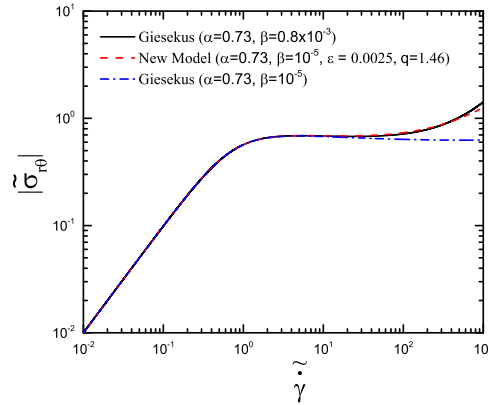


FIG. 1. Influence of the CCR-like term on the homogeneous flow curve.

worth mentioning that the CCR-like term accounts for nontrivial normal stress differences at large shear rates. In summary, the results confirm that the CCR-like term, which incorporates a power-law prefactor accounting for polymer stretch, is a good choice.

Fig. 2 shows the effects of mobility factor  $\alpha$ , ratio of the characteristic relaxation times  $\varepsilon$ , and power-law parameter  $q$  on the behavior of the homogeneous flow curve. We find that the slope after the plateau is affected by the value of  $\alpha$  (see Fig. 2(a)). For all values of  $\alpha$  used in this study, the flow curve is monotonic. Increasing the value of  $\alpha$  decreases the slope. Fig. 2(b) illustrates that parameter  $\varepsilon$  determines where the upturn of the shear stress occurs. As this parameter, i.e., the relative importance of the CCR-like term, is increased, the upturn is shifted to smaller shear rates.

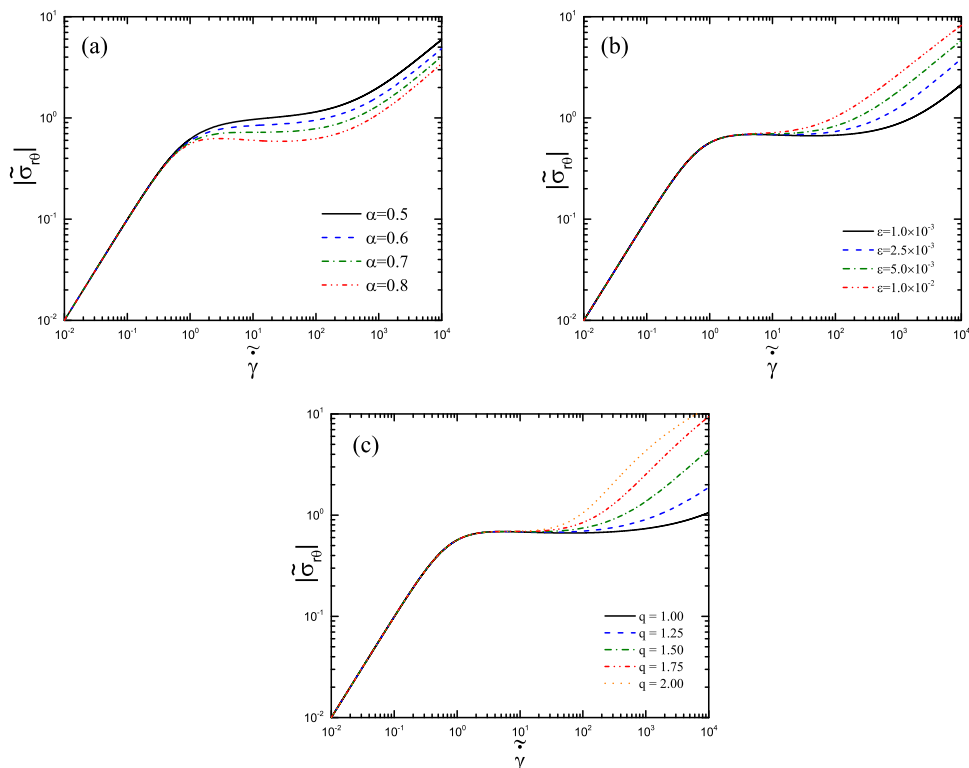


FIG. 2. Effects of (a)  $\alpha$  with  $q = 1.46$  and  $\varepsilon = 2.5 \times 10^{-4}$ , (b)  $\varepsilon$  with  $\alpha = 0.73$  and  $q = 1.46$ , and (c)  $q$  with  $\alpha = 0.73$  and  $\varepsilon = 2.5 \times 10^{-4}$  on the homogeneous flow curve. Parameter  $\beta$  was kept fixed at  $10^{-5}$ .

Fig. 2(c) shows that the slope of the shear stress is determined by power-law parameter  $q$  at large shear rates. Increasing the value of  $q$  leads to an increase in the slope. This parameter determines the influence of chain stretch, as the trace of the conformation tensor is a relative measure of this quantity.

## B. Start-up of cylindrical Couette flow

Next, we proceed with the inhomogeneous flow calculations. We consider the start-up of a simple shear flow. The temporal evolution of the azimuthal velocity at the inner wall is specified by<sup>4</sup>

$$\tilde{v}_\theta(r^* = 0, \tilde{t}) = Wi \tanh(\tilde{a}\tilde{t}), \quad (35)$$

where  $\tilde{a}$  is the dimensionless ramp rate of the rheometer. Typically,  $\tilde{a}$  lies in the range of  $O(10^0-10^2)$ . Note that the azimuthal velocity at the inner cylinder corresponds to the apparent shear rate across the gap at steady state,<sup>4</sup> i.e.,  $\tilde{\gamma}_{app} = Wi$ . The outer cylinder is assumed to be stationary; therefore, we set  $\tilde{v}_\theta(r^* = 1) = 0$ . No flow through the walls is specified by setting the normal components of the total and differential velocities equal to zero ( $\tilde{v}_r = \Delta v_r = 0$ ). To specify no slip along the walls, the tangential component of the differential velocity must vanish at the boundaries ( $\Delta \tilde{v}_\theta = 0$ ).

The parameters that could not be determined by fitting the steady homogeneous flow curve were estimated for the inhomogeneous flow calculations as follows. To avoid long running times, a moderate local diffusivity constant ( $\tilde{D} = 10^{-3}$ ) and a fast ramp rate ( $\tilde{a} = 100$ ) were used. A moderate value of  $\tilde{D}_{nonloc} = 10^{-3}$  was selected to remove the sharp kink in the banded profiles. Because inertial effects were not the main focus of this work, we simply set  $E^{-1} = 10^{-5}$ . The dimensionless curvature was specified as  $q^* = 0.04$ , which is a typical value for cylindrical Couette experiments. To observe pronounced bands, we used a large value of the molecular weight ratio of  $\chi = 0.1$ . As in Ref. 18, the total initial concentration corresponded to  $\mu = 0.1$ .

The flow problem was solved using the numerical procedure employed in Germann *et al.*<sup>5,39,43</sup> We used a Chebyshev pseudospectral collocation method<sup>44,45</sup> with  $N_1 = 200$  collocation points for spatial discretization and a second-order Crank–Nicolson scheme<sup>46</sup> with an adaptive time step for temporal discretization. The nonlinear system of the discretized algebraic equations was iteratively solved at each time step by using an inverse-based multilevel incomplete lower-upper (ILU) preconditioned Newton–Krylov solver.<sup>43</sup> The key feature of the inverse-based multilevel ILU preconditioner is that the magnitude of the preconditioned coefficient matrix perturbations with respect to the identity matrix can be controlled by adjusting the magnitude of the inverse triangular factors during the construction of the coefficient matrix. The theoretical details of this special ILU preconditioner can be found in Bollhöfer and Saad<sup>47</sup> and Bollhöfer *et al.*<sup>48</sup>

To check the convergence of the numerical calculations, we repeated the simulation obtained for  $Wi = 10$  with  $N_2 = 150$  and  $N_3 = 250$  collocation points. For each grid of collocation points, the solution was computed at 100 different radial positions that were equally spaced across the cylindrical gap. The error between the state variables computed on grids  $N_1 = 200$  and those computed on grids  $N_2$  and  $N_3$  was never larger than  $8.23 \times 10^{-6}$ . If the values were larger than unity, the relative error was considered, otherwise, the absolute error was taken into account.<sup>49</sup>

Figs. 3(a) and 3(b) display the effect of the Weissenberg number on the steady-state profiles of the total azimuthal velocity and polymer number density, respectively. The velocity profile shows two distinct shear bands for the range  $3 \lesssim Wi \lesssim 63$ . Increasing the Weissenberg number moves the kink separating the two bands from the rotating inner wall to the stationary outer wall. Because of the two-fluid coupling between flow and concentration, the profile of the polymer number density is also banded. Note that the total mass/number density of the polymeric solution is assumed to be constant, whereas the individual mass/number densities are allowed to vary. This is in contrast to the predictions obtained for one-fluid polymer models, which do not take diffusional effects into account. Moreover, we find that the curvature of the cylindrical Couette geometry justifies the curved profile of the polymer number density.

Steady-state profiles of the nontrivial stress components are shown across the cylindrical gap in Figs. 4(a)–4(c) for different values of the Weissenberg number. The magnitudes of these components are larger for greater Weissenberg numbers. As required by the relatively small gap

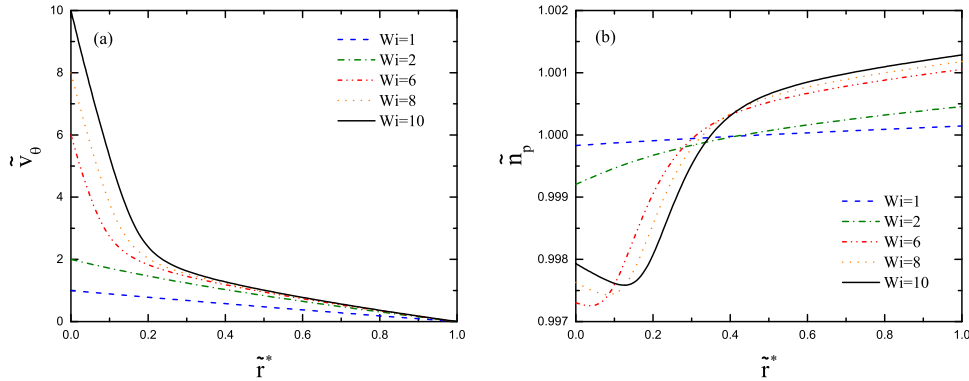


FIG. 3. Profiles of the (a) velocity and (b) polymer number density calculated for different Weissenberg numbers. The values of the other model parameters used in the calculation are  $\alpha = 0.73$ ,  $\varepsilon = 2.5 \times 10^{-3}$ ,  $q = 1.46$ ,  $\beta = 10^{-5}$ ,  $E^{-1} = 10^{-5}$ ,  $\bar{D} = \bar{D}_{nonloc} = 10^{-3}$ ,  $\chi = 0.1$ , and  $\mu = 0.1$ .

and the Cauchy momentum balance in Eq. (29), the absolute value of the shear stress reduces linearly from the inner rotating wall to the outer stationary wall (see Fig. 4(a)). The profiles of the  $rr$ - and  $\theta\theta$ -components of the stress tensor are given in Figs. 4(b) and 4(c), respectively. As expected, the  $\theta\theta$ -component is much larger in magnitude than the  $rr$ -component. In the nonlinear regime, the strong nonlinearities in these two profiles are related to shear banding. Furthermore, we note that the  $zz$ -component is identically zero. Daprà and Scarpi<sup>50</sup> analytically solved the Giesekus model for steady cylindrical Couette flow and investigated the spatial behavior of the nontrivial stress components in the gap. In their work, the value of  $\alpha$  was restricted to  $\alpha < 0.5$ , as the Giesekus model does not have a real physical solution outside this range for high Weissenberg numbers.<sup>51,52</sup>

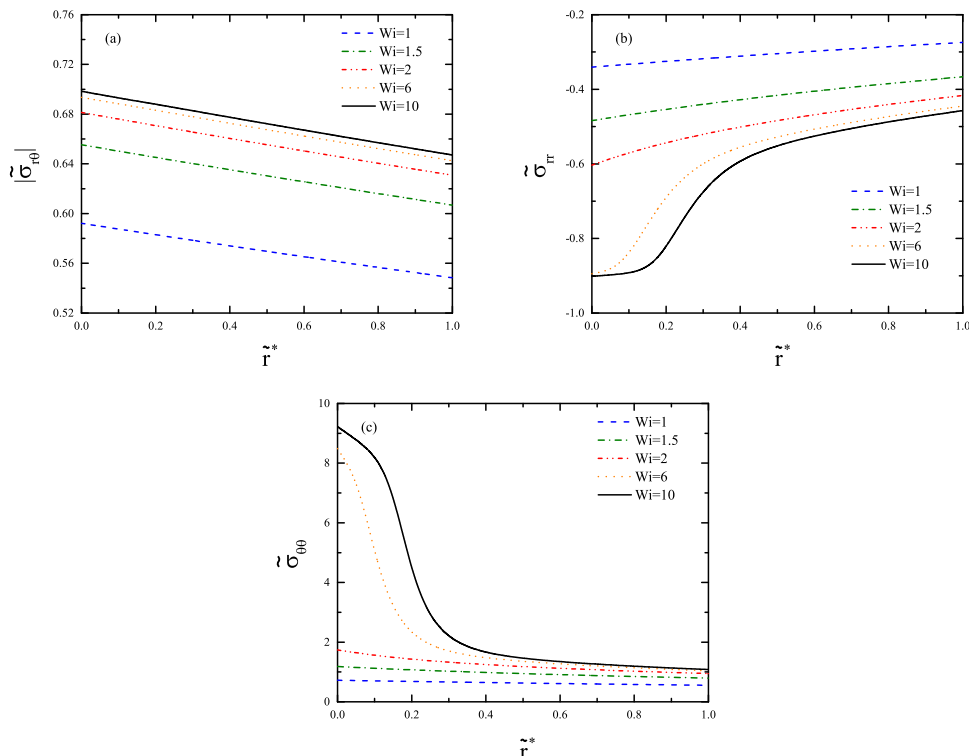


FIG. 4. Profiles of the (a) shear stress, (b) radial stress, and (c) tangential stress across the cylindrical gap calculated for different values of the Weissenberg number. The other model parameters are the same as those given in the caption of Fig. 3.

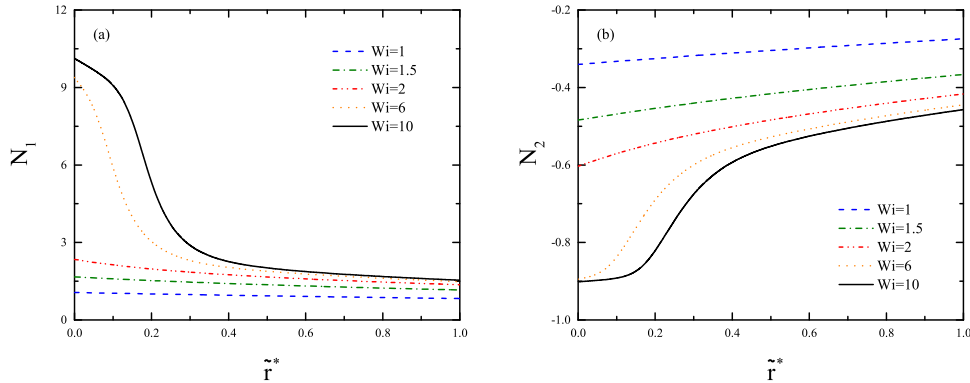


FIG. 5. Profiles of the (a) first and (b) second normal stress differences across the cylindrical gap calculated for different values of the Weissenberg number. The other model parameters are the same as those given in the caption of Fig. 3.

By adding a large solvent contribution or a second nonlinear relaxation term, this limitation can be overcome.

Figs. 5(a) and 5(b) display the profiles of the first and second normal stress differences, respectively, across the gap width for different Weissenberg numbers. As the first normal stress difference is defined as  $N_1 = \bar{\sigma}_{\theta\theta} - \bar{\sigma}_{rr}$ , Fig. 5(a) is obtained by subtracting the results shown in Fig. 4(b) from those shown in Fig. 4(c). Furthermore, as the  $zz$ -component is identically zero, the results of the second normal stress difference,  $N_2 = \bar{\sigma}_{rr} - \bar{\sigma}_{zz}$ , are exactly the same as those depicted in Fig. 4(b).

Fig. 6 shows the influence of the stress-induced migration on the steady-state profile of the polymer number density. The calculation was performed with and without the term accounting for stress-induced migration. The horizontal line indicates that without this term, the polymer number density is nearly constant across the cylindrical gap. Stress-induced migration is clearly responsible for the formation of the shear bands. As we used homogeneous initial conditions, standard Fickian diffusion has no significant effect.

Fig. 7 displays the effects of the total polymer concentration and ratio of the solvent molecular weight to the polymer molecular weight on the steady-state profile of the polymer number density. As expected from experiments,<sup>22,53</sup> Fig. 7(a) shows that increasing the total polymer concentration causes the shear bands to be more pronounced. This is because the polymer concentration appears in the expression for the extra stress provided in Eq. (32). Consequently, larger polymer concentrations cause a greater extra stress and thus more shear-induced migration. At this early stage of the work, we did not consider any functional dependencies of the material parameters. Laboratory experiments will have to be conducted in a future study to work out some of these scaling laws, such

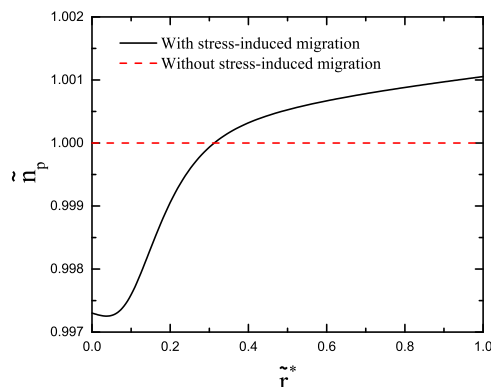


FIG. 6. Number density of the polymer calculated for the model with and without the term corresponding to stress-induced migration. The values of the model parameters used in the calculation are  $\alpha = 0.73$ ,  $\varepsilon = 2.5 \times 10^{-3}$ ,  $q = 1.46$ ,  $\beta = 10^{-5}$ ,  $E^{-1} = 10^{-5}$ ,  $\bar{D} = \bar{D}_{nonloc} = 10^{-3}$ ,  $\chi = 0.1$ ,  $\mu = 0.1$ , and  $Wi = 6$ .

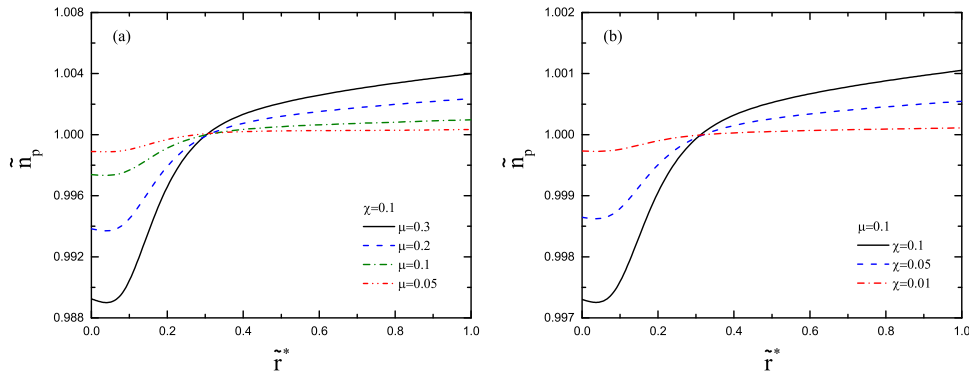


FIG. 7. Influences of the (a) total polymer concentration and (b) molecular weight ratio on the number density of the polymer. The other model parameters are the same as those given in the caption of Fig. 6.

as the effect of the polymer concentration on mobility factor  $\alpha$ . Fig. 7(b) shows that increasing the molecular weight ratio leads to more pronounced shear bands. However, experimental data show the opposite trend.<sup>22,53</sup> This discrepancy can be explained by the fact that as the parameters determining the shape of the flow curve are fixed, the results displayed in Fig. 7(b) only provide information about the impact of the molecular weight ratio on the diffusional processes. Experimental studies on shear banding have observed values for  $\chi$  of  $O(10^{-5})$ .<sup>22</sup> To observe pronounced effects, we decided to continue with the rather large value of  $\chi = 0.1$ .

Fig. 8 displays the influence of the local diffusivity constant. The steady-state profile of the polymer number density (see Fig. 8(a)) was found to be independent of the local diffusivity

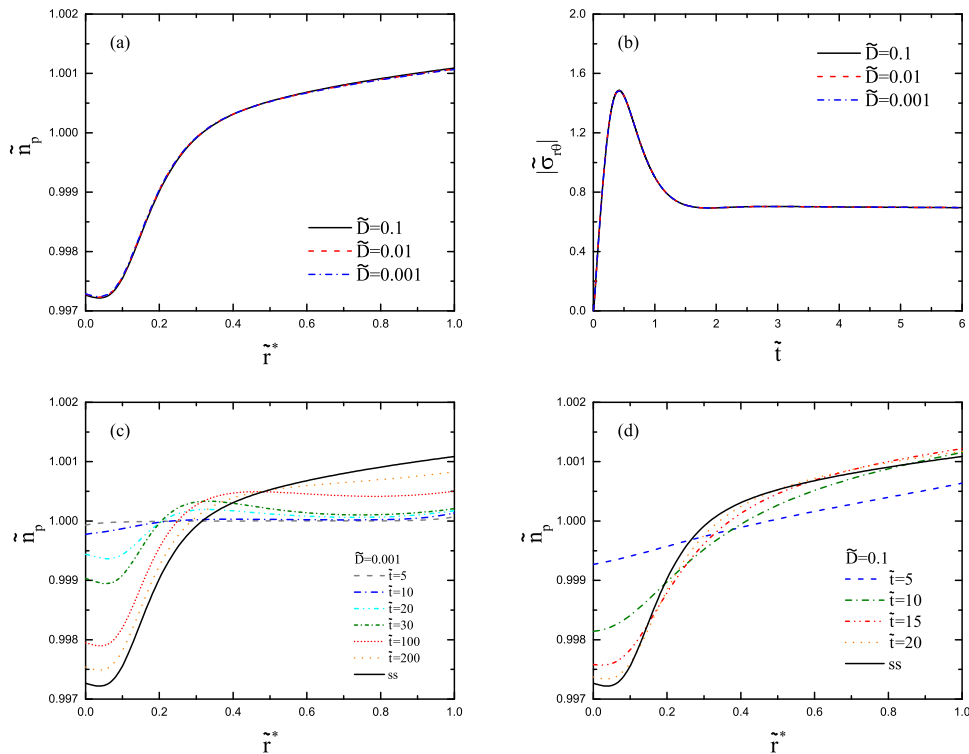


FIG. 8. Effect of the local diffusivity constant on the (a) the steady-state profile of the polymer density, (b) temporal behavior of the absolute value of the shear stress at the inner wall, and (c) and (d) the temporal behavior of the polymer number density profile in the cylindrical gap. The other model parameters are the same as those given in the caption of Fig. 6.



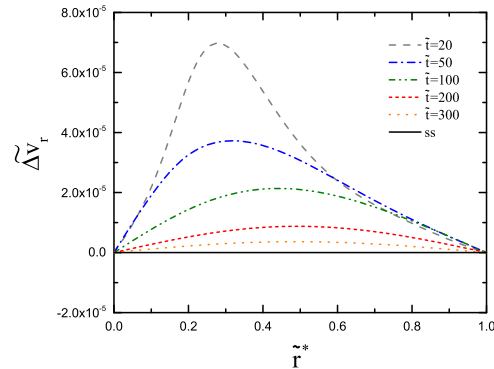


FIG. 9. Temporal evolution of the radial component of the differential velocity across the gap width calculated with  $Wi = 10$ . The other model parameters are the same as those given in the caption of Fig. 6.

constant. As opposed to Cromer *et al.* model,<sup>34</sup> our model predicts a steady-state solution whose smoothness is not affected by this parameter. In Fig. 8(b), we display the transient evolution of the absolute value of the wall shear stress. For a sufficiently high ramp rate, the nonlinear Giesekus relaxation generates an overshoot that triggers shear-band formation. A smaller value for the diffusivity constant increases the time to reach steady state. As the flow curve is monotonic and the shear stress is determined by Cauchy momentum balance, Eq. (29), the local diffusivity constant does not have a significant effect on the shear stress. However, some differences can be observed in the microstructural quantities (see Figs. 8(c) and 8(d)). For  $\tilde{D} = 10^{-3}$  shown in Fig. 8(c), up to  $\tilde{t} = 50$ , the transient profiles of the polymer number density intersect at a unique position in the gap where the shear bands separate. Thereafter, nonlocal stress diffusion pushes the kink toward the outer cylinder.

Fig. 9 shows the temporal evolution of the radial component of the differential velocity in the cylindrical gap width. We find that this component increases to a maximum and then decreases to zero as steady-state is achieved. Note that the azimuthal component is of much smaller magnitude and therefore does not have an effect on the computational results. The profile of the radial component is different to predictions of a two-fluid model for shear banding wormlike micelles.<sup>39</sup> As this model is based on the assumption that the wormlike micelles form shear bands as a result of their dynamic breakage, the radial velocity develops a local extremum at the transition region of the shear bands.

Fig. 10 shows the effect of the nonlocal diffusivity constant on the velocity profile. The speciality of our two-fluid model is that the smoothness of the profiles is controlled solely by this

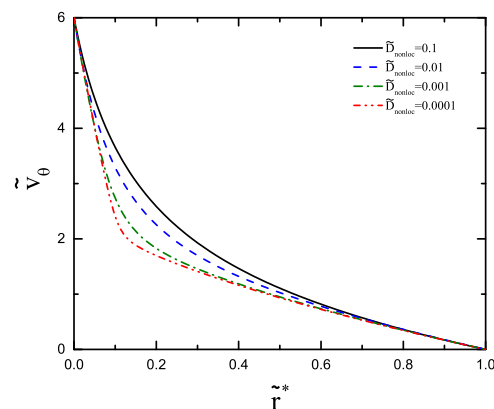


FIG. 10. Effect of the nonlocal diffusivity constant on the steady-state profile of the velocity. The other model parameters are the same as those given in the caption of Fig. 6.

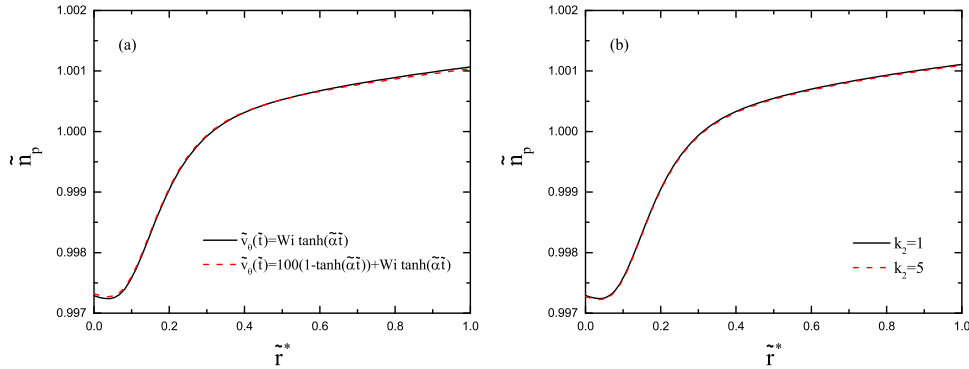


FIG. 11. (a) Steady-state profiles of the polymer number density calculated using different deformation histories where ramp-up ( $\tilde{v}_\theta(\tilde{t}) = Wi \tanh(\tilde{a}\tilde{t})$ ) and ramp-down ( $\tilde{v}_\theta(\tilde{t}) = 100(1 - \tanh(\tilde{a}\tilde{t})) + Wi \tanh(\tilde{a}\tilde{t})$ ) conditions were applied. The terminal value of  $Wi$  was set to six. (b) Steady-state profiles of the polymer number density calculated using differently perturbed initial conditions. The model parameters are the same as those given in the caption of Fig. 6.

parameter. We find that a larger value of  $\tilde{D}_{nonloc}$  leads to a smoother steady-state solution. Although the uniqueness of the solution is guaranteed here even if  $\tilde{D}_{nonloc} = 0$ , there may well be a parameter space where this may not be the case.

Figs. 11(a) and 11(b) show the impact of the deformation history and initial condition, respectively, on the steady-state profile of the polymer number density. To investigate the influence of deformation history, we performed some ramp-up and ramp-down tests. We started the ramp-up test from rest; for the ramp-down test, the steady-state solution at  $Wi = 100$  was used as the initial condition. The terminal value of  $Wi$  was specified to be six. We find that the steady-state solution displayed in Fig. 11(a) is independent of the deformation history. To examine the impact of the initial condition, we started the simulation using an initial polymer density perturbed by  $\tilde{n}_p = 1 + k_1 \cos(\pi k_2 y / (R_o - R_i))$  with a magnitude of  $k_1 = 10^{-3}$  and two wave numbers of  $k_2 = 1$  and  $k_2 = 5$ . Fig. 11(b) shows that the different initial conditions evolved into a unique steady-state profile. As in the model of Cromer *et al.*<sup>34</sup> and as observed in experiments,<sup>18</sup> our model is capable of predicting a unique banded steady-state that is independent of the initial condition and the applied deformation history.

#### IV. CONCLUSION

In this work, we developed a new two-fluid model for semi-dilute entangled polymer solutions using the generalized bracket approach of nonequilibrium thermodynamics. The new model is based on the hypothesis that diffusional processes are responsible for steady-state shear banding in semi-dilute entangled polymer solutions. A recently developed two-fluid approach<sup>5,39</sup> was used to describe Fickian diffusion and stress-induced migration in the polymer solution. Although stress diffusion is accounted for in this two-fluid approach, an additional stress-diffusive term had to be included in the conformation tensor equation to control the smoothness of the profiles. The advantage of this two-fluid approach is that the differential velocity is treated as a state variable. Consequently, the additional boundary conditions arising from the higher diffusive derivatives in the time evolution equation of the differential velocity can be directly imposed with respect to this variable. For instance, no-slip and no-flux boundary conditions translate into the requirement that the tangential and normal components, respectively, of the differential velocity must be zero at the boundaries. Another advantage is that the total mass is conserved by the model equations themselves. Therefore, it is no longer necessary to explicitly impose a no-flux condition on the polymer concentration to prevent outflow material through the system boundaries. The time evolution equation for the conformation tensor includes a nonlinear Giesekus relaxation, which accounts for the stress overshoot of a shear-banding material during the rapid start-up of a simple shear flow. To capture the upturn of the flow curve at high shear rates, we developed a nonlinear relaxation term

that resembles the term used in the Rolie-Poly model to account for CCR and chain stretch. Because our model is relatively simple, it is an ideal candidate for use in more complicated flow simulations. To investigate the general behavior of the new model, we solved the model for cylindrical Couette flow. We found that the steady-state solution is unique for different initial conditions and independent of the applied deformation history. Furthermore, we observed that stress-induced migration is responsible for shear-band formation. The results of this study encourage us to analyze the model behavior in other types of inhomogeneous flows. Furthermore, more experimental research is needed to verify the hypothesis in the model that shear band formation is triggered by diffusion.

## ACKNOWLEDGMENTS

Financial support from the Max Buchner Research Foundation is gratefully acknowledged.

## APPENDIX: NON-DIMENSIONALIZATION

The dimensionless forms of Eqs. (24), (33)–(34), and (29)–(32) using the scalings introduced in Sec. II A are as follows:

$$E^{-1} \frac{\partial \tilde{\mathbf{v}}}{\partial \tilde{t}} = -E^{-1} \tilde{\mathbf{v}} \cdot \tilde{\nabla} \tilde{\mathbf{v}} - \tilde{\nabla} \tilde{p} + \tilde{\nabla} \cdot \tilde{\boldsymbol{\sigma}}, \quad (\text{A1})$$

$$E^{-1} \frac{\chi \tilde{n}_s \tilde{n}_p}{(\tilde{n}_p + \chi \tilde{n}_s)^2} \left( \frac{\partial}{\partial \tilde{t}} + \tilde{\mathbf{v}} \cdot \tilde{\nabla} \right) (\tilde{\Delta} \mathbf{v}) = \frac{\chi \tilde{n}_s}{\tilde{n}_p + \chi \tilde{n}_s} \left\{ -\tilde{\nabla} \tilde{n}_p + \tilde{\nabla} \cdot \tilde{\boldsymbol{\sigma}}^p \right\} \\ - \frac{\tilde{n}_p}{\tilde{n}_p + \chi \tilde{n}_s} \left\{ -\tilde{\nabla} \tilde{n}_s + \beta \tilde{\nabla}^2 \tilde{\mathbf{v}}^s \right\} - \tilde{D} \tilde{\Delta} \mathbf{v}, \quad (\text{A2})$$

$$\frac{\partial \tilde{n}_p}{\partial \tilde{t}} = -\tilde{\nabla} \cdot (\tilde{\mathbf{v}}^p \tilde{n}_p), \quad (\text{A3})$$

$$\frac{\partial \tilde{\mathbf{c}}}{\partial \tilde{t}} = -\tilde{\mathbf{v}}^p \cdot \tilde{\nabla} \tilde{\mathbf{c}} + \tilde{\mathbf{c}} \cdot \tilde{\nabla} \tilde{\mathbf{v}}^p + (\tilde{\nabla} \tilde{\mathbf{v}}^p)^T \cdot \tilde{\mathbf{c}} \\ - [(1 - \alpha) \mathbf{I} + \alpha \tilde{\mathbf{c}}] (\tilde{\mathbf{c}} - \mathbf{I}) \\ + \varepsilon (\text{tr} \tilde{\mathbf{c}} - 3)^q (\tilde{\mathbf{c}} - \mathbf{I}) \\ + \tilde{D}_{nonloc} \left( \tilde{\mathbf{c}} \cdot \tilde{\nabla} (\tilde{\nabla} \cdot \tilde{\boldsymbol{\sigma}}^p) + [\tilde{\nabla} (\tilde{\nabla} \cdot \tilde{\boldsymbol{\sigma}}^p)]^T \cdot \tilde{\mathbf{c}} \right), \quad (\text{A4})$$

$$\tilde{\boldsymbol{\sigma}} = \tilde{\boldsymbol{\sigma}}^p + \beta \left[ \tilde{\nabla} \tilde{\mathbf{v}}^s + (\tilde{\nabla} \tilde{\mathbf{v}}^s)^T \right] = \tilde{n}_p (\tilde{\mathbf{c}} - \mathbf{I}) + \beta \left[ \tilde{\nabla} \tilde{\mathbf{v}}^s + (\tilde{\nabla} \tilde{\mathbf{v}}^s)^T \right], \quad (\text{A5})$$

$$\tilde{\mathbf{v}}^p = \tilde{\mathbf{v}} + \frac{\chi \tilde{n}_s}{\tilde{n}_p + \chi \tilde{n}_s} \tilde{\Delta} \mathbf{v}, \quad (\text{A6})$$

$$\tilde{\mathbf{v}}^s = \tilde{\mathbf{v}} - \frac{\tilde{n}_p}{\tilde{n}_p + \chi \tilde{n}_s} \tilde{\Delta} \mathbf{v}. \quad (\text{A7})$$

<sup>1</sup> P. D. Olmsted, "Perspectives on shear banding in complex fluids," *Rheol. Acta* **47**(3), 283–300 (2008).

<sup>2</sup> S. Manneville, "Recent experimental probes of shear banding," *Rheol. Acta* **47**(3), 301–318 (2008).

<sup>3</sup> T. Divoux, M. A. Fardin, S. Manneville, and S. Lerouge, "Shear banding of complex fluids," *Annu. Rev. Fluid Mech.* **48**, 81–103 (2016).

<sup>4</sup> L. Zhou, P. A. Vasquez, L. P. Cook, and G. H. McKinley, "Modeling the inhomogeneous response and formation of shear bands in steady and transient flows of entangled liquids," *J. Rheol.* **52**(2), 591–623 (2008).

<sup>5</sup> N. Germann, L. P. Cook, and A. N. Beris, "Investigation of the inhomogeneous shear flow of a wormlike micellar solution using a thermodynamically consistent model," *J. Non-Newton. Fluid Mech.* **207**, 21–31 (2014).

<sup>6</sup> P. A. Vasquez, G. H. McKinley, and L. P. Cook, "A network scission model for wormlike micellar solutions: I. Model formulation and viscometric flow predictions," *J. Non-Newton. Fluid Mech.* **144**(2–3), 122–139 (2007).

<sup>7</sup> N. Germann, L. P. Cook, and A. N. Beris, "Nonequilibrium thermodynamic modeling of the structure and rheology of concentrated wormlike micellar solutions," *J. Non-Newton. Fluid Mech.* **196**, 51–57 (2013).

<sup>8</sup> M. Grmela, F. Chinesta, and A. Ammar, "Mesoscopic tube model of fluids composed of worm-like micelles," *Rheol. Acta* **49**, 495–506 (2010).

<sup>9</sup> L. Zhou, L. P. Cook, and G. H. McKinley, "Probing shear-banding transitions of the VCM model for entangled wormlike micellar solutions using large amplitude oscillatory shear (LAOS) deformations," *J. Non-Newton. Fluid Mech.* **165**(21), 1462–1472 (2010).

- <sup>10</sup> L. Zhou, L. P. Cook, and G. H. McKinley, "Multiple shear-banding transitions for a model of wormlike micellar solutions," *SIAM J. Appl. Math.* **72**(4), 1192–1212 (2012).
- <sup>11</sup> M. Doi and S. F. Edwards, *The Theory of Polymer Dynamics* (Oxford University Press, 1988), Vol. 73.
- <sup>12</sup> A. E. Likhtman and R. S. Graham, "Simple constitutive equation for linear polymer melts derived from molecular theory: Rolie–Poly equation," *J. Non-Newton. Fluid Mech.* **114**(1), 1–12 (2003).
- <sup>13</sup> J. M. Adams and P. D. Olmsted, "Nonmonotonic models are not necessary to obtain shear banding phenomena in entangled polymer solutions," *Phys. Rev. Lett.* **102**(6), 067801 (2009).
- <sup>14</sup> J. M. Adams, S. M. Fielding, and P. D. Olmsted, "Transient shear banding in entangled polymers: A study using the Rolie–Poly model," *J. Rheol.* **55**(5), 1007–1032 (2011).
- <sup>15</sup> R. L. Moorcroft and S. M. Fielding, "Criteria for shear banding in time-dependent flows of complex fluids," *Phys. Rev. Lett.* **110**(8), 086001 (2013).
- <sup>16</sup> R. L. Moorcroft and S. M. Fielding, "Shear banding in time-dependent flows of polymers and wormlike micelles," *J. Rheol.* **58**(1), 103–147 (2014).
- <sup>17</sup> S. Ravindranath, S. Q. Wang, M. Olechnowicz, and R. P. Quirk, "Banding in simple steady shear of entangled polymer solutions," *Macromolecules* **41**(7), 2663–2670 (2008).
- <sup>18</sup> S. Cheng and S. Q. Wang, "Is shear banding a metastable property of well-entangled polymer solutions?," *J. Rheol.* **56**(6), 1413–1428 (2012).
- <sup>19</sup> P. E. Boukany and S. Q. Wang, "Shear banding or not in entangled DNA solutions depending on the level of entanglement," *J. Rheol.* **53**(1), 73–83 (2009).
- <sup>20</sup> Y. Li, M. Hu, G. B. McKenna, C. J. Dimitriou, G. H. McKinley, R. M. Mick, D. C. Venerus, and L. A. Archer, "Flow field visualization of entangled polybutadiene solutions under nonlinear viscoelastic flow conditions," *J. Rheol.* **57**(5), 1411–1428 (2013).
- <sup>21</sup> M. Harvey and T. A. Waigh, "Optical coherence tomography velocimetry in controlled shear flow," *Phys. Rev. E* **83**(3), 031502 (2011).
- <sup>22</sup> S. Jaradat, M. Harvey, and T. A. Waigh, "Shear-banding in polyacrylamide solutions revealed via optical coherence tomography velocimetry," *Soft Matter* **8**(46), 11677–11686 (2012).
- <sup>23</sup> K. A. Dill and B. H. Zimm, "A rheological separator for very large DNA molecules," *Nucleic Acids Res.* **7**(3), 735–749 (1979).
- <sup>24</sup> M. J. MacDonald and S. J. Muller, "Experimental study of shear-induced migration of polymers in dilute solutions," *J. Rheol.* **40**(2), 259–283 (1996).
- <sup>25</sup> A. B. Metzner, Y. Cohen, and C. Rangel-Nafaile, "Inhomogeneous flows of non-Newtonian fluids: Generation of spatial concentration gradients," *J. Non-Newton. Fluid Mech.* **5**, 449–462 (1979).
- <sup>26</sup> S. Fielding and P. D. Olmsted, "Early stage kinetics in a unified model of shear-induced demixing and mechanical shear banding instabilities," *Phys. Rev. Lett.* **90**(22), 224501 (2003).
- <sup>27</sup> E. Helfand and G. H. Fredrickson, "Large fluctuations in polymer solutions under shear," *Phys. Rev. Lett.* **62**(21), 2468 (1989).
- <sup>28</sup> N. Clarke and T. C. B. McLeish, "Shear flow effects on phase separation of entangled polymer blends," *Phys. Rev. E* **57**(4), R3731 (1998).
- <sup>29</sup> S. T. Milner, "Hydrodynamics of semidilute polymer solutions," *Phys. Rev. Lett.* **66**(11), 1477 (1991).
- <sup>30</sup> M. Doi and A. Onuki, "Dynamic coupling between stress and composition in polymer solutions and blends," *J. Phys. II* **2**(8), 1631–1656 (1992).
- <sup>31</sup> J. L. Goveas and G. H. Fredrickson, "Curvature-driven shear banding in polymer melts," *J. Rheol.* **43**(5), 1261–1277 (1999).
- <sup>32</sup> A. N. Beris and B. J. Edwards, *Thermodynamics of Flowing Systems with Internal Microstructure*, Oxford Engineering Science Series Vol. 36 (Oxford University Press, 1994).
- <sup>33</sup> M. V. Apostolakis, V. G. Mavrantzas, and A. N. Beris, "Stress gradient-induced migration effects in the Taylor–Couette flow of a dilute polymer solution," *J. Non-Newton. Fluid Mech.* **102**(2), 409–445 (2002).
- <sup>34</sup> M. Cromer, M. C. Villet, G. H. Fredrickson, and L. G. Leal, "Shear banding in polymer solutions," *Phys. Fluids* **25**(5), 051703 (2013).
- <sup>35</sup> M. Cromer, M. C. Villet, G. H. Fredrickson, L. G. Leal, R. Stepanyan, and M. J. H. Bulters, "Concentration fluctuations in polymer solutions under extensional flow," *J. Rheol.* **57**(4), 1211–1235 (2013).
- <sup>36</sup> M. Cromer, G. H. Fredrickson, and L. G. Leal, "A study of shear banding in polymer solutions," *Phys. Fluids* **26**(6), 063101 (2014).
- <sup>37</sup> A. N. Beris and V. G. Mavrantzas, "On the compatibility between various macroscopic formalisms for the concentration and flow of dilute polymer solutions," *J. Rheol.* **38**(5), 1235–1250 (1994).
- <sup>38</sup> J. W. van Egmond and G. G. Fuller, "Concentration fluctuation enhancement in polymer solutions by extensional flow," *Macromolecules* **26**(26), 7182–7188 (1993).
- <sup>39</sup> N. Germann, L. P. Cook, and A. N. Beris, "A differential velocities-based study of diffusion effects in shear-banding micellar solutions," *J. Non-Newton. Fluid Mech.* **232**, 43–54 (2016).
- <sup>40</sup> A. Leygue, A. N. Beris, and R. Keunings, "A constitutive equation for entangled linear polymers inspired by reptation theory and consistent with non-equilibrium thermodynamics," *J. Non-Newton. Fluid Mech.* **101**(1), 95–111 (2001).
- <sup>41</sup> S. M. Fielding and P. D. Olmsted, "Flow phase diagrams for concentration-coupled shear banding," *Eur. Phys. J. E: Soft Matter Biol. Phys.* **11**(1), 65–83 (2003).
- <sup>42</sup> W. H. Press, S. A. Teukolsky, W. T. Vetterling, and B. P. Flannery, *Numerical Recipes* (Cambridge University Press, 1992).
- <sup>43</sup> N. Germann, M. Dressler, and E. J. Windhab, "Numerical solution of an extended White–Metzner model for eccentric Taylor–Couette flow," *J. Comput. Phys.* **230**(21), 7853–7866 (2011).
- <sup>44</sup> R. G. Voigt, D. Gottlieb, and M. Y. Hussaini, *Spectral Methods for Partial Differential Equations* (SIAM, Philadelphia, 1984).
- <sup>45</sup> R. Peyret, *Spectral Methods for Incompressible Viscous Flow* (Springer Science & Business Media, 2002), Vol. 148.

- <sup>46</sup> R. D. Richtmyer and K. W. Morton, *Difference Methods for Initial Value Problems: Interscience Tracts in Pure and Applied Mathematics* (Interscience Publishers, 1967).
- <sup>47</sup> M. Bollhöfer and Y. Saad, "Multilevel preconditioners constructed from inverse-based ILUs," *SIAM J. Sci. Comput.* **27**(5), 1627–1650 (2006).
- <sup>48</sup> M. Bollhöfer, Y. Saad, and O. Schenk, ILUPACK-Preconditioning Software Package, Release 2.2, 2008, <http://www-public.tu-bs.de/bolle/ilupack/>.
- <sup>49</sup> U. M. Ascher and C. Greif, *A First Course on Numerical Methods* (SIAM, 2011), Vol. 7.
- <sup>50</sup> I. Daprà and G. Scarpi, "Analytical solution for a Couette flow of a Giesekus fluid in a concentric annulus," *J. Non-Newton. Fluid Mech.* **223**, 221–227 (2015).
- <sup>51</sup> G. Schleiniger and R. J. Weinacht, "Steady Poiseuille flows for a Giesekus fluid," *J. Non-Newton. Fluid Mech.* **40**(1), 79–102 (1991).
- <sup>52</sup> J. Y. Yoo and H. Ch. Choi, "On the steady simple shear flows of the one-mode Giesekus fluid," *Rheol. Acta* **28**(1), 13–24 (1989).
- <sup>53</sup> S. Q. Wang, S. Ravindranath, and P. E. Boukany, "Homogeneous shear, wall slip, and shear banding of entangled polymeric liquids in simple-shear rheometry: A roadmap of nonlinear rheology," *Macromolecules* **44**(2), 183–190 (2011).